Studies of the photoionization cross sections of acetylene

D. Lynch, M.-T. Lee,[a] R. R. Lucchese,[b] and V. McKoy

Arthur Amos Noyes Laboratory of Chemical Physics,[c] California Institute of Technology, Pasadena, California 91125

(Received 5 July 1983; accepted 5 August 1983)

We have studied the photoionization cross sections and photoelectron asymmetry parameters for all molecular orbitals of acetylene. These cross sections were obtained using accurate frozen-core Hartree–Fock continuum orbitals in the final-state wave function. The Hartree–Fock continuum equations were solved using the iterative Schwinger variational method. These fixed-nuclei cross sections are compared with available experimental data and with results obtained using the Stieltjes moment theory approach and the continuum multiple scattering method. The possible role of a shape resonance in the $1\pi_u \rightarrow k\pi_g$ channel and the resonant structure of the σ_u continuum are discussed in some detail.

I. INTRODUCTION

Recent experimental[1–6] and theoretical[7–9] studies have shown that shape resonances play a major role in molecular photoionization. Shape resonances lead to important effects in the photoionization cross sections and photoelectron angular distributions. For example, such resonances can induce large deviations of the vibrational branching ratios from those based on Franck–Condon factors. To date, studies have shown that the Hartree–Fock approximation can provide a very useful quantitative description of these shape resonant effects in molecular photoionization cross sections.[8–14]

In this paper we present the results of our studies of the photoionization cross sections of acetylene and, in particular, of the role of shape resonances in these cross sections. The cross sections are obtained from the direct solution of the electron–molecular ion collisional equations in the frozen-core Hartree–Fock (FCHF) approximation at the ground state equilibrium geometry of acetylene. The continuum Hartree–Fock equations were solved by the iterative Schwinger method[15] which we have used in our earlier studies of the photoionization of N_2,[16] CO_2,[17] NO,[18] and CO.[19]

We have obtained the photoionization cross sections and photoelectron asymmetry parameters for the valence molecular orbitals ($1\pi_u$, $3\sigma_g$, $2\sigma_u$, and $2\sigma_g$) and for the K-shell orbitals ($1\sigma_g$ and $1\sigma_u$) of acetylene. These results are compared with available experimental data[6,20–23] and with results obtained using the Stieltjes–Tchebycheff moment theory (STMT) approach[24] and the continuum multiple scattering model.[21,22] Of particular interest in C_2H_2 is the double bump structure around 14 eV in the $^2\Pi_u$ photoionization spectrum. Several recent experimental[6,20–22,25,26] and theoretical[20,21,26,27] studies have addressed the question of the nature of the underlying resonances in this region, e.g., to what extent is this structure due to shape or autoionizing resonances or to some combination of such resonances. Although no firm understanding of this resonant excitation mechanism has yet emerged, it seems certain that the autoionizing $^1\Pi_u(2\sigma_u \rightarrow 1\pi_g)$ valence state contributes to the structure in this region.[6,20] The present results show that, while the $1\pi_u \rightarrow k\sigma_g$ and $k\delta_g$ one-electron continua are nonresonant in this region, the cross section could be significantly enhanced by a shape resonance in the $1\pi_u \rightarrow k\pi_g$ continuum around 13 eV. This interpretation depends very critically on the question of the location of the $^1\Sigma_u^+(1\pi_u \rightarrow 1\pi_g)$ state in acetylene. Electronic structure calculations indicate that this transition lies just above the $1\pi_u$ ionization threshold and, in fact, causes the shape resonance in the $1\pi_u \rightarrow k\pi_g$ continuum. This is quite different from the analogous situation in N_2 where the $^1\Sigma_u^+(1\pi_u \rightarrow 1\pi_g)$ state is known to lie well into the discrete region of the spectrum and hence the $k\pi_g$ continuum function can be constructed orthogonal to the $1\pi_g$ orbital.[16,28] Final-state correlation effects must play an important role in any quantitative interpretation of the resonant structure in this region.

As expected, the σ_u photoionization continuum of acetylene is shape-resonance enhanced. The cross sections and eigenphase sums for this continuum show some interesting features. For example, the eigenphase sums indicate that there are two shape resonances in this channel. Around a photoelectron kinetic energy of 2 eV the first shape resonance has a pronounced effect on the cross section and asymmetry parameter for ionization out of the $3\sigma_g$ level. This shift in shape resonant activity from a photoelectron kinetic energy of about 15 eV in N_2 to 2 eV in C_2H_2 is consistent with the changes in nuclear separations and confirms the trends previously seen in the measured cross sections[20] and in the STMT calculations.[24] The second shape resonance feature is much broader, lies at higher energy, and is not noticeable in the vibrationally unresolved cross sections and angular distributions for the $3\sigma_g$ level. However, the effects of both this resonance and the lower energy one are very evident in the $2\sigma_g$ photoionization cross sections. The effects of these shape resonances on the valence shell and K-shell cross sections are discussed in some detail.

II. METHOD

The rotationally unresolved, fixed-nuclei photoionization cross section is given by

[a] Present address: Instituto de Quimica, Universidade Federal de São Carlos, São Carlos, S. P. Brasil.

[b] Present address: Bell Laboratories, Murray Hill, New Jersey 07974.

[c] Contribution No.: 6841.

 0021-9606/84/051907-10$02.10

$$\sigma(R) = \frac{4\pi^2\omega}{3} \left|\langle \Psi_i(\mathbf{r},R) \left| \mu \right| \Psi_f(\mathbf{r},R)\rangle\right|^2 , \quad (1)$$

where μ is the dipole moment operator and ω the photon frequency. In Eq. (1) $\Psi_i(\mathbf{r},R)$ is the initial state of the molecule and $\Psi_f(\mathbf{r},R)$ the final ionized state. In these studies the final state wave function is obtained using the frozen-core Hartree–Fock (FCHF) approximation. In this approximation the final state is described by a single electronic configuration in which the ionic core orbitals are constrained to be identical to the HF orbitals of the neutral molecule and the continuum orbital hence satisfies the one-electron Schrödinger equation

$$\left[-\tfrac{1}{2}\nabla^2 + V_{N-1}(\mathbf{r},R) - \frac{k^2}{2}\right]\phi_{\mathbf{k}}(\mathbf{r},R) = 0 , \quad (2)$$

where $(k^2/2)$ is the photoelectron kinetic energy and $\phi_{\mathbf{k}}$ satisfies the appropriate boundary conditions. The key step in the study of molecular photoionization cross sections at any level of approximation is the determination of these Hartree–Fock continuum functions, $\phi_{\mathbf{k}}$.

To obtain the continuum orbital $\phi_{\mathbf{k}}$ it is convenient to work with the integral form of Eq. (2). The partial wave components of $\phi_{\mathbf{k}}$, which are defined by the expansion

$$\phi_{\mathbf{k}}^{(-)}(\mathbf{r}) = \left(\frac{2}{\pi}\right)^{1/2} \sum_{l=0}^{l_p} \sum_{m=-l}^{l} i^l \psi_{klm}^{(-)}(\mathbf{r})\, Y_{lm}^*(\Omega_{\hat{k}}) , \quad (3)$$

then satisfy the Lippmann–Schwinger equation

$$\psi_{klm}^{(-)} = S_{klm} + G_c^{(-)} U \psi_{klm}^{(-)} , \quad (4)$$

where $G_c^{(-)}$ is the Coulomb Green's function with incoming-wave boundary conditions, $U = 2V$ where V is the molecular ion potential, V_{N-1}, with the Coulomb component removed, and S_{klm} is the appropriate partial wave Coulomb function. In Eq. (3) an infinite sum over l has been truncated at $l = l_p$. We have recently developed an iterative approach to the solution of Eq. (4) which is based on the Schwinger variational principle.[15,29] Applications[16–19] have shown that the method is an effective approach to the determination of these continuum solutions for molecular ion potentials. Details have been discussed elsewhere[15] and here we will discuss only a few essential features of the method. In this approach we first solve the Lippman–Schwinger equation by assuming an approximate separable form for the scattering potential U,

$$U(\mathbf{r},\mathbf{r}') \cong U^S(\mathbf{r},\mathbf{r}') = \sum_{\alpha_i,\alpha_j} \langle \mathbf{r} \left| U \right| \alpha_i\rangle (U^{-1})_{ij} \langle \alpha_j \left| U \right| \mathbf{r}'\rangle , \quad (5)$$

where the matrix $(U^{-1})_{ij}$ is the inverse of the matrix with elements $U_{ij} = \langle \alpha_i \left| U \right| \alpha_j\rangle$. With this approximate potential, U^S, the solutions of Eq. (4) are simply

$$\psi_{klm}^{(0)}(\mathbf{r}) = S_{klm}(\mathbf{r}) + \sum_{\alpha_i,\alpha_j} \langle \mathbf{r} \left| G_c^{(-)} U \right| \alpha_i\rangle \times (D^{-1})_{ij} \langle \alpha_j \left| U \right| S_{klm}\rangle , \quad (6)$$

where

$$D_{ij} = \langle \alpha_i \left| U - U G_c^{(-)} U \right| \alpha_j\rangle . \quad (7)$$

The use of a separable potential of the form of Eq. (5) in the solution of the Lippmann–Schwinger equation for $\psi_{klm}^{(0)}$ can be shown to be equivalent to using the functions $\alpha_i(\mathbf{r})$ in the Schwinger variational principle for collisions.[30] At this stage these functions can be chosen to be entirely discrete basis functions such as Cartesian or spherical Gaussian functions which are known to be very effective in representing the multicenter nature of molecular electronic eigenfunctions.[31]

With suitable basis sets, the solutions $\psi_{klm}^{(0)}$ can already provide quantitatively reliable photoionization cross sections which, moreover, can be shown to be variationally stable at the Hartree–Fock level.[19] We have, however, also developed an iterative procedure for obtaining the converged solutions of Eq. (2). The details of this approach are discussed elsewhere.[29] The results presented in this paper were generally calculated with continuum functions obtained after two steps in the iterative procedure.

For the initial state Ψ_i of Eq. (1), we generally use the SCF wave function but, in certain cases, we will include some effects due to electron correlation by using a configuration interaction wave function. In addition to the dipole length form given in Eq. (1) we also obtain cross sections and asymmetry parameters in the dipole velocity form. The difference between these two forms of the cross section can generally be viewed as a measure of electron correlation effects.[32]

III. RESULTS

The ground state electronic configuration of acetylene is $1\sigma_g^2 1\sigma_u^2 2\sigma_g^2 2\sigma_u^2 3\sigma_g^2 1\pi_u^4$. The SCF wave function for the neutral C_2H_2 molecule was constructed from a $[3s\,2p\,|\,2s]$ Cartesian Gaussian basis set contracted from a primitive $(9s\,5p\,|\,4s)$ basis[31] augmented with a set of d and p polarization functions on the C and H centers, respectively. The exponent for the d function was 0.75 and 1.0 for the p function. The calculations were done at the equilibrium geometry with C–C and C–H bond lengths of 2.2734 and 2.003 a.u., respectively. The SCF energy with this basis and geometry is $-76.831\,406$ a.u.

To obtain the final state one-electron continuum functions used in these studies, the various matrix elements associated with Eq. (6) must be evaluated. All matrix elements were computed by a single-center expansion technique with radial integrals obtained using a Simpson's rule quadrature. Detailed discussions of the numerical methods used have been given elsewhere.[16,17] The various partial wave expansion parameters were chosen as follows:

(1) Maximum partial wave included in the expansion of the scattering solution $= l_p = 10(\sigma_g, \pi_g)$, $11(\sigma_u, \pi_u)$, and $8(\delta_g)$;

(2) Maximum partial wave retained in the expansion of the occupied orbitals in the direct potential $= l_i^{\mathrm{dir}} = 30$;

(3) Maximum partial wave retained in the expansion

TABLE I. Starting basis sets for solution of Eq. (6).

Symmetry of continuum solution	Center	l	m	
σ_g	H	0	0	1.0, 0.5, 0.25
		1	0	1.0, 0.5, 0.25
	C	0	0	4.0, 2.0, 1.0, 0.5, 0.25
		1	0	1.0, 0.5, 0.25
		2	0	1.0, 0.5, 0.25
	Origin	0	0	4.0, 2.0
		2	0	1.0
		4	0	0.5
		6	0	0.5
σ_u	H	0	0	1.0, 0.5, 0.25
		1	0	1.0, 0.5, 0.25
	C	0	0	4.0, 2.0, 1.0, 0.5
		1	0	1.0, 0.5
		2	0	1.0, 0.5
	Origin	1	0	4.0, 2.0
		3	0	1.0
		5	0	0.5
		7	0	0.5
π_u	H	1	1	1.0, 0.5, 0.25
		2	1	0.5
	C	1	1	1.0, 0.5, 0.25
		2	1	1.0, 0.5, 0.25
	Origin	1	1	1.0, 0.5
		3	1	1.0, 0.5
		5	1	0.5
π_g	H	1	1	1.0, 0.5, 0.25
		2	1	0.5
	C	1	1	1.0, 0.5, 0.25
		2	1	1.0, 0.5
	Origin	2	1	1.0
		4	1	0.5
		6	1	0.5
δ_g	H	2	2	1.0, 0.5, 0.25
		3	2	0.5
	C	2	2	1.0, 0.5, 0.25
		3	2	1.0, 0.5, 0.25
	Origin	2	2	1.0, 0.5
		4	2	1.0, 0.5
		6	2	0.5

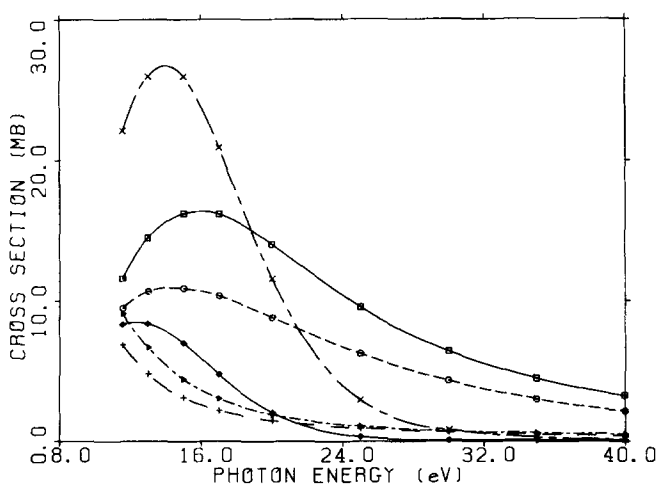

FIG. 1. The $1\pi_u \rightarrow k\sigma_g$, $k\pi_g$, and $k\delta_g$ partial channel photoionization cross sections for $C_2H_2^+$ (dipole length and dipole velocity forms): ⊟⊟⊟, $1\pi_u \rightarrow k\delta_g$ (length); ⊖⊖, $1\pi_u \rightarrow k\delta_g$ (velocity); —▷ – –▷—, $1\pi_u \rightarrow k\sigma_g$ (length); —+—, $1\pi_u \rightarrow k\sigma_g$ (velocity); —× – –×—, $1\pi_u \rightarrow k\pi_g$ (length); —◇———◇—, $1\pi_u \rightarrow k\pi_g$ (velocity).

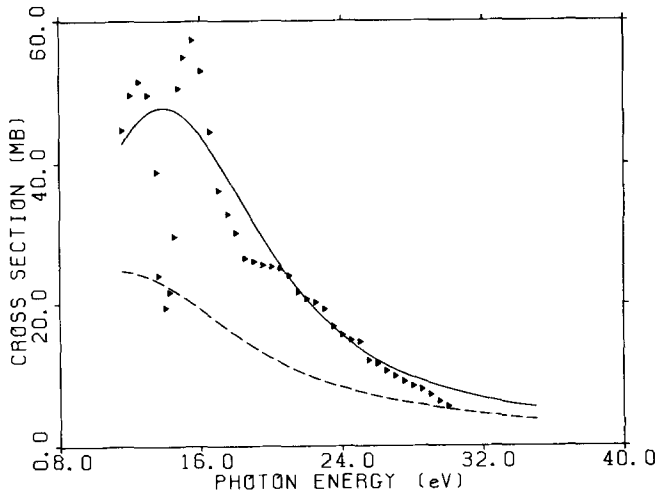

FIG. 2. Photoionization cross sections for the $X\,^2\Pi_u$ state of $C_2H_2^+$: —, present results using the dipole length form; ---, dipole velocity form; ▶, experimental results (Ref. 20) normalized to the dipole length cross sections at 24 eV.

of the occupied orbitals in the exchange terms $= l_i^{ex}$ $= 20(1\sigma_g)$, $12(2\sigma_g)$, $12(3\sigma_g)$, $19(1\sigma_u)$, $11(2\sigma_u)$, and $11(1\pi_u)$;

(4) Maximum partial wave retained in the expansion of $1/r_{12}$ in the direct potential $= \lambda_m^{dir} = 60$;

(5) Maximum partial wave retained in the expansion of $1/r_{12}$ in the exchange terms $= \lambda_m^{ex} = 30$.

All other partial wave expansions were truncated at $l = 30$. For the radial integrations, the grid contained 1000 points and extended to 79 a.u. with the smallest step size being 0.01 a.u. and the largest step size 0.16 a.u.

Table I lists the initial basis sets used in Eq. (6) for each symmetry. The basis set contained spherical Gaussian functions, defined by

$$\alpha(\mathbf{r}) = N_{\gamma,l,m} |\mathbf{r}-\mathbf{A}|^l \exp(-\gamma|\mathbf{r}-\mathbf{A}|^2) Y_{lm}(\Omega_{\mathbf{r}-\mathbf{A}}) \,. \quad (8)$$

A. The $X\,^2\Pi_u$ state

In photoionization leading to the $X^2\Pi_u$ state of $C_2H_2^+$, an electron is ejected from the $1\pi_u$ orbital into a continuum orbital of σ_g, π_g, or δ_g symmetry. We take the ionization potential for this channel to be 11.4 eV.[33] Figure 1 shows the $k\sigma_g$, $k\pi_g$, and $k\delta_g$ components of this cross section obtained using continuum functions which are solutions of the appropriate static-exchange potential for the singlet-coupled final states, e.g., $^1\Sigma_u^+(1\pi_u^3 k\pi_g)$. Results using continuum solutions obtained after one iteration and a Hartree–Fock initial wave function are shown. In Fig. 2 we compare the calculated total cross sections with the synchrotron radiation measurements of Unwin and Bradshaw.[20] This data has been normalized to our calculated dipole length cross sections at a photon energy of 24 eV.

A comparison of the cross sections in Fig. 2 shows clearly that the double bump structure around 14 eV is due to autoionizing resonances, the effects of which are not included in the present calculations. This structure

has been interpreted previously in terms of autoionization,[6,20] but our results indicate that the prominent peaks around 13 and 15 eV are due to one, or possibly two, autoionizing resonances interacting with a shape-resonance enhanced background continuum. This is essentially the interpretation of these features recently given by Parr *et al.*[6] in which the autoionizing transitions were identified as $3\sigma_g \rightarrow n\sigma_u$ and $2\sigma_u \rightarrow 1\pi_g$ at around 13.3 and 15.5 eV, respectively. We note that the $3\sigma_g \rightarrow n\sigma_u(^1\Sigma_u^+)$ and $2\sigma_u \rightarrow 1\pi_g(^1\Pi_u)$ transitions will be coupled to the $1\pi_u \rightarrow k\pi_g(^1\Sigma_u^+)$ and $1\pi_u \rightarrow k\sigma_g$, $k\delta_g(^1\Pi_u)$ continua, respectively. Recently, Levine and Soven,[34] using a time-dependent local-density approximation to the RPA, accounted for the 15.5 eV peak and about half of the peak at around 13 eV assuming a single $2\sigma_u \rightarrow 1\pi_g$ autoionizing resonance. In this model substantial intensity is shifted from below the ionization threshold into the continuum due to electron correlation. This view differs from our present suggestion that the $1\pi_g \rightarrow n\pi_g$ state already lies in the continuum at the Hartree–Fock level of approximation.

The cross sections of Fig. 1 show the shape-resonance enhancement of the π_g continuum. This enhancement is due to the "$1\pi_u \rightarrow 1\pi_g$" transition which lies in the continuum, at least in the Hartree–Fock approximation. No definitive assignment of an intravalence $^1\Sigma_u^+(1\pi_u \rightarrow 1\pi_g)$ transition has yet been made in the discrete spectrum of acetylene. If such a transition does lie well below the $^2\Pi_u$ ionization threshold, then the enhancement of the $1\pi_u \rightarrow k\pi_g$ cross sections in Fig. 2 could be an artifact of our Hartree–Fock description of the final state wave function in which electron correlation effects are neglected. This is exactly what happens in the $1\pi_u \rightarrow k\pi_g$ continuum of N_2 where the $^1\Sigma_u^+(1\pi_u \rightarrow 1\pi_g)$ intravalence state is clearly spuriously pushed into the continuum in the Hartree–Fock approximation.[28] In Refs. 16 and 28 this deficiency of the Hartree–Fock potential was removed by constructing the $k\pi_g$ continuum to be orthogonal to the valence-like $1\pi_g$ orbital of

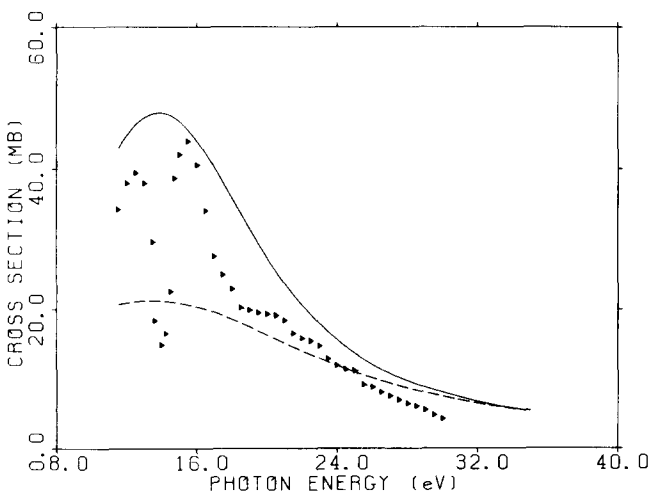

FIG. 3. Comparison of the dipole length cross sections for the $X\ ^2\Pi_u$ state of $C_2H_2^+$ using the singlet and triplet potentials to obtain the $1\pi_u \rightarrow k\pi_g$ component: —, singlet potential; --- triplet potential, experimental results (Ref. 20) normalized to the triplet potential results at 24 eV.

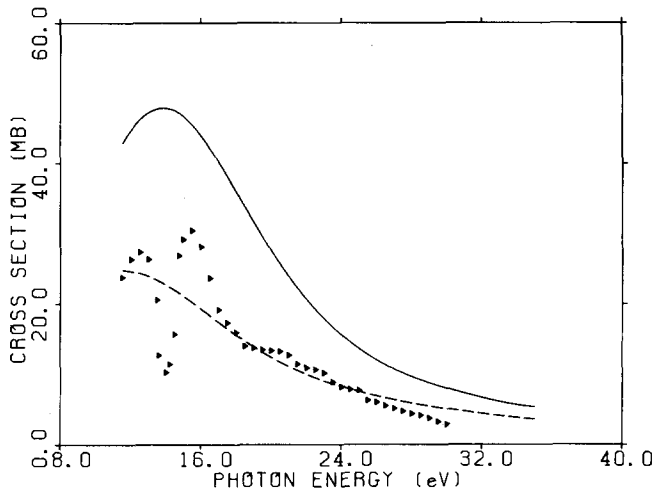

FIG. 4. Photoionization cross sections for the $X\ ^2\Pi_u$ state of $C_2H_2^+$ (same labels as in Fig. 2 but with the experimental data normalized to the dipole velocity results at 24 eV).

the $^3\Sigma_u^+(1\pi_u \rightarrow 1\pi_g)$ state. As expected, the resulting cross section was substantially reduced and, in fact, was essenitally equivalent to those obtained using the $k\pi_g$ continuum of the static-exchange potential of the $^3\Sigma_u^+(1\pi_u \rightarrow 1\pi_g)$ state, i.e., the triplet potential. Figure 3 compares the cross sections for the $^2\Pi_u$ state in which the $k\pi_g$ contribution was obtained with continuum solutions of the singlet and triplet potentials. With the use of the triplet potential all evidence of the shape resonance has disappeared and the corresponding cross section has been reduced to a very small value. The use of the triplet $k\pi_g$ continuum is extreme since we have seen that it is virtually equivalent to orthogonalization to a very valence-like π_g orbital of the $^3\Sigma_u^+(1\pi_u^3 1\pi_g)$ state which lies at around 5.2 eV.[35] The $^1\Sigma_u^+(1\pi_u^3 1\pi_g)$ state lies at higher energy and its π_g orbital can be substantially different from that of the triplet state. In fact, extensive RPA calculations give a valence-like $^1\Sigma_u^+$ state at 12.95 eV with an oscillator strength of about 0.5.[36] This result indicates that the valence-like $^1\Sigma_u^+$ state may actually be in the $^2\Pi_u$ continuum or, if not, at least close to its threshold. The probable role of final-state correlation effects on this shape resonance along with the autoionizing features in this same spectral region will make studies of these cross sections both challenging and fruitful. Absolute measurements of these cross sections would be useful.

A comparison of the results of Figs. 1 and 2 obtained with the dipole length and velocity forms of the oscillator strength again shows that electron correlation effects are important in these photoionization cross sections. Such effects are expected to be more pronounced in the $k\pi_g$ subchannel than in the $k\sigma_g$ and $k\delta_g$. The difference between these two forms of the cross sections is substantial even out at a photon energy of 24 eV where the experimental results of Ref. 20 were normalized to the length form of the calculated cross sections in Fig. 2. With this choice of normalization, the autoionizing feature around 15 eV has a cross section close to 60 Mb while Fig. 4 shows that a similar nor-

malization to the velocity cross sections at 24 eV gives the same feature a cross section of about 30 Mb. Although the synchrotron radiation measurements of Unwin and Bradshaw[20] are relative, the absolute cross sections in this spectral region have been studied with conventional light sources.[25,37,38] The measurements of Walker and Weissler[37] and of Schoen[38] both give a value of about 60 Mb for the cross section for the autoionizing feature at 15 eV, whereas Metzger and Cook[25] report a value of about 37 Mb. The discrepancy between these two measurements is large enough that one cannot unambiguously decide, on this basis, which normalization of Unwin *et al.* data, e.g., to the calculated length cross sections of Fig. 2 or 3, leads to the correct cross sections. This is unfortunate since such a comparison would tell whether the $1\pi_u \rightarrow k\pi_g$ shape resonance feature in the cross sections of Fig. 2 is spurious or not. However, a comparison of the relative data of Unwin *et al.*[20] with the measurements of Refs. 25, 37, and 38 does suggest that the normalized cross sections of Fig. 1 are probably closer to the correct ones. Such a conclusion would indicate that the $k\pi_g$ continuum is shape resonant.

In Fig. 5 we compare our calculated photoionization cross sections with those of the continuum multiple scattering model.[21] There are clearly substantial differences between these two sets of cross sections which arise primarily from the $k\pi_g$ and $k\delta_g$ continua. In the π_g continuum this difference must be due to the sensitivity of the cross section on the implied location of the $1\pi_u \rightarrow 1\pi_g$ transition relative to threshold. Differences in the $1\pi_u \rightarrow k\delta_g$ component result more directly from the approximate potentials assumed in the multiple scattering model.

Figure 6 compares the $1\pi_u^{-1}$ cross sections obtained by the Stieltjes moment theory method[24] with our calculated cross sections of Fig. 3. In these moment theory calculations the $1\pi_u \rightarrow k\pi_g$ contribution was obtained with the triplet-coupled potential, a procedure we have shown to be essentially equivalent to orthogonalizing the singlet π_g continuum functions to the valence-like $1\pi_g$ orbital.[16,28] Moreover, the $1\pi_u \rightarrow k\delta_g$ partial channel cross section was also calculated with the triplet potential since the singlet potential appropriate to the $1\pi_u^3 k\delta_g$ configuration is not expressible in terms of the usual Coulomb and exchange operators when real valued molecular orbitals are used. The moment theory calculations[24] were performed using standard bound state computer codes which require that all potentials be expressible in terms of the usual J and K operators. In our cross sections of Fig. 3 the π_g contribution is obtained with the triplet potential but for the δ_g component we used the correct singlet-coupled potential. The significant difference at low energy between the present cross sections and those of the moment theory occurs in the δ_g component. In fact, the use of the triplet potential in this channel has led to a peak in the cross section around 12 to 13 eV which is not present if the correct singlet potential is used and which fortuitously coincides with the first peak of the double bump structure observed around 13 eV.

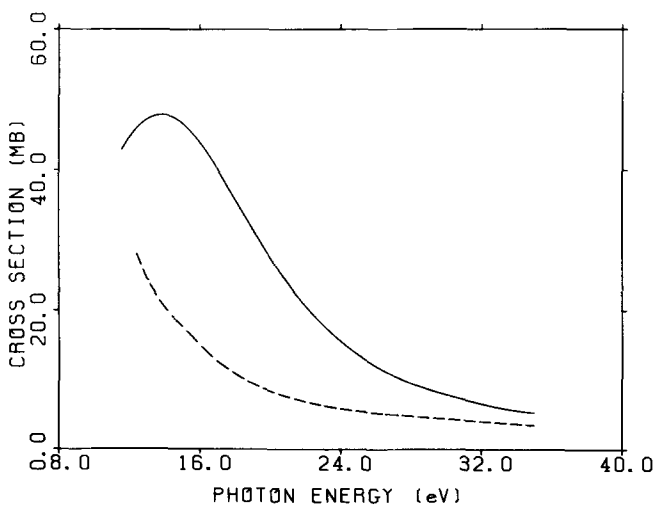

FIG. 5. Calculated cross sections for the $X^2\Pi_u$ state of $C_2H_2^+$: —, present results with the dipole length form and the singlet potential to obtain the $1\pi_u \rightarrow k\pi_g$ component; ---, multiple scattering model (Ref. 21).

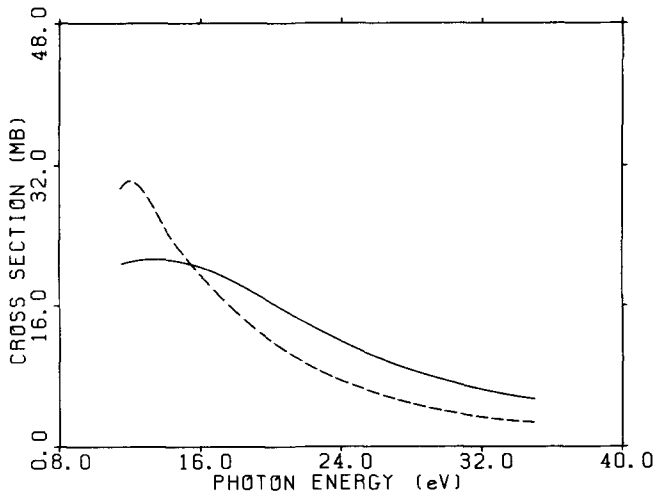

FIG. 6. Calculated cross sections for the $X^2\Pi_u$ state of $C_2H_2^+$: —, present results using the triplet potential for the $1\pi_u \rightarrow k\pi_g$ component (dipole length form); ---, Stieltjes moment theory results (Ref. 24).

In Fig. 7 we compare our calculated asymmetry parameters for the $1\pi_u$ orbital with the measured values of Parr *et al.*[6] for the $\nu_2 = 0$ vibrational band and with the multiple scattering results of Ref. 22. For clarity, we do not show the complete set of data actually reported in Ref. 6. We also choose to compare our fixed-nuclei results with the measured values of the $\nu_2 = 0$ band since this is the dominant vibrational transition. The calculated asymmetry parameters do not show the strong dip around 14 eV seen in the measured data and which is clearly due to an autoionizing resonance. Characteristically of photoionization of a π orbital the calculated parameters rise rapidly from a low value near threshold to a value of about unity at higher energy. The calculated parameters are obtained with the singlet-coupled potential. The pa-

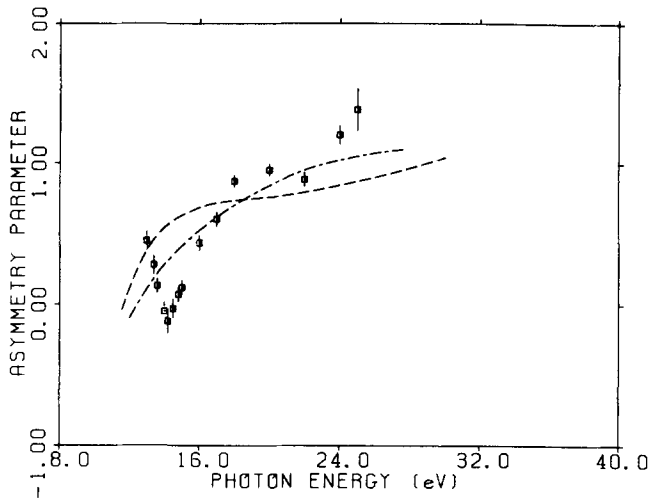

FIG. 7. Photoelectron asymmetry parameters for the $X\,^2\Pi_u$ state of $C_2H_2^+$: ——, present results using the singlet potential for the $1\pi_u \rightarrow k\pi_g$ component (dipole length form); – – – –, multiple scattering results (Ref. 22); □, experimental results ($\nu_2 = 0$; Ref. 6).

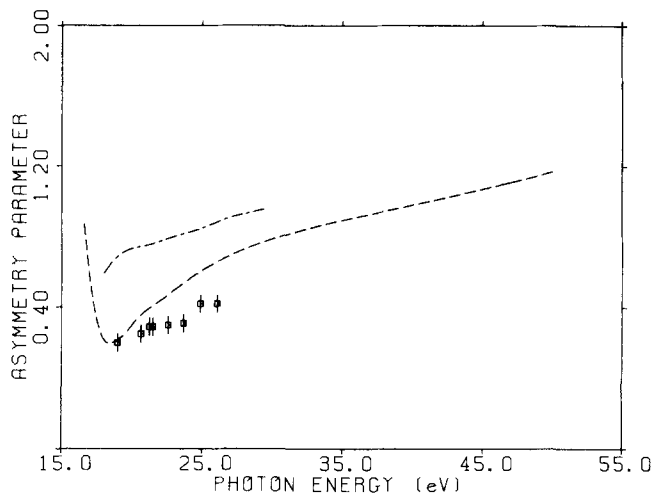

FIG. 9. Photoelectron asymmetry parameters for the $A\,^2\Sigma_g^+$ state of $C_2H_2^+$: ——, present results (dipole length form); – · –, multiple scattering results (Ref. 22); □, experimental results (Ref. 22).

rameters obtained with the triplet potential are similar in shape to those of Fig. 7 but notably smaller in magnitude between threshold and 20 eV.

B. The $A\,^2\Sigma_g^+$ state

In the one-electron picture used here the $A\,^2\Sigma_g^+$ channel corresponds to photoionization from the $3\sigma_g$ orbital into the σ_u or π_u continuum. Figure 8 shows the calculated photoionization cross sections using continuum solutions obtained after one iteration and a Hartree–Fock initial state wave function. The use of a correlated initial state wave function changed these cross sections only slightly and hence, for this and the remaining channels, we will discuss only the results

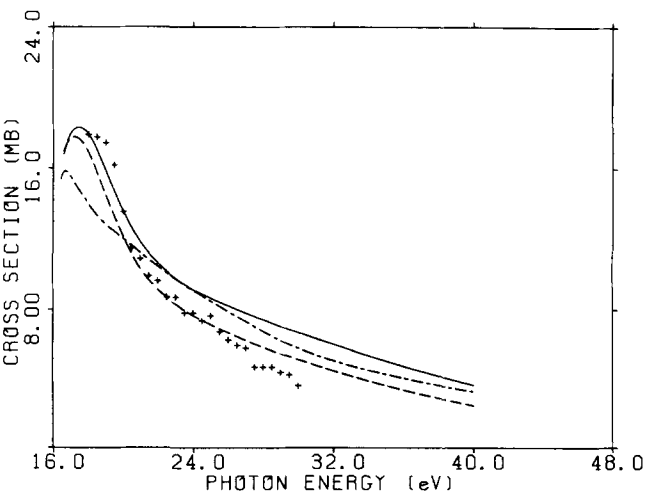

FIG. 8. Photoionization cross section for the $A\,^2\Sigma_g^+$ state of $C_2H_2^+$: ——, present results (dipole length form); – – –, present results (dipole velocity form); – · –, Stieltjes moment theory results (Ref. 24); +, experimental results (Ref. 20) normalized to our dipole length cross sections at 20 eV.

obtained with a Hartree–Fock initial state. In Fig. 8 we also show the synchrotron radiation measurements of Unwin and Bradshaw[20] normalized to the calculated dipole length cross sections at a photon energy of 20 eV. Our photon energy scale assumes the experimental ionization potential of 16.4 eV.[33]

The sharp feature in these cross sections just above threshold is caused by the shape resonance in the σ_u continuum. This behavior is clearly analogous to that of the $3\sigma_g \rightarrow k\sigma_u$ channel in N_2 and, moreover, the shift in the shape resonant activity from a photoelectron kinetic energy of 15 eV in N_2 to about 2 eV in C_2H_2 is consistent with the changes in nuclear separations of these two molecules. With the experimental data arbitrarily normalized to the calculated values at 24 eV, our peak cross sections near threshold are obviously too low. The difference between the calculated and observed cross sections in this important region clearly depends on where this normalization is carried out. Absolute measurements of these cross sections would be useful. Our cross sections and those of the Stieltjes theory method[24] show the same overall behavior.

The calculated asymmetry parameters of Fig. 9 show the expected dip near threshold and agree quite well with the measurements of Keller[22] which unfortunately do not extend to low enough energy to show the rapid change in β predicted near threshold. Extension of these measurements to lower energies would be desirable. The β values based on the multiple scattering model[22] do not agree very well with either our calculated values or with the experimental data.[22]

In Fig. 10 we show the calculated eigenphase sum for the σ_u continuum of this $A\,^2\Sigma_g^+$ ion. The rapid increase in this eigenphase sum between threshold and around 21 eV is obviously due to the shape resonance responsible for the pronounced features in both the fixed-nuclei cross section and asymmetry parameters

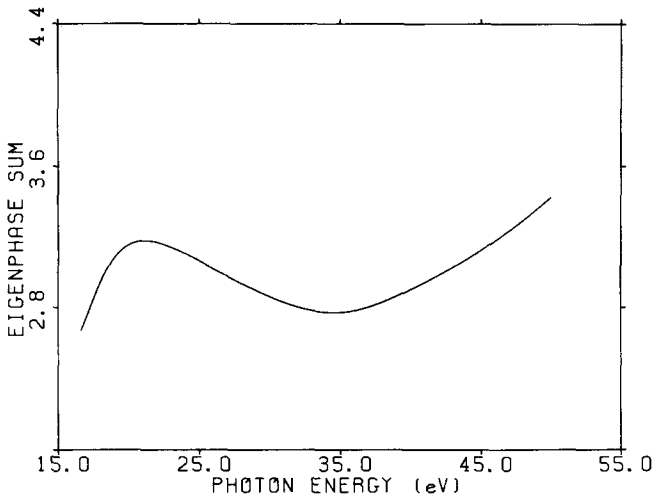

FIG. 10. Eigenphase sum for the $3\sigma_g \rightarrow k\sigma_u$ component.

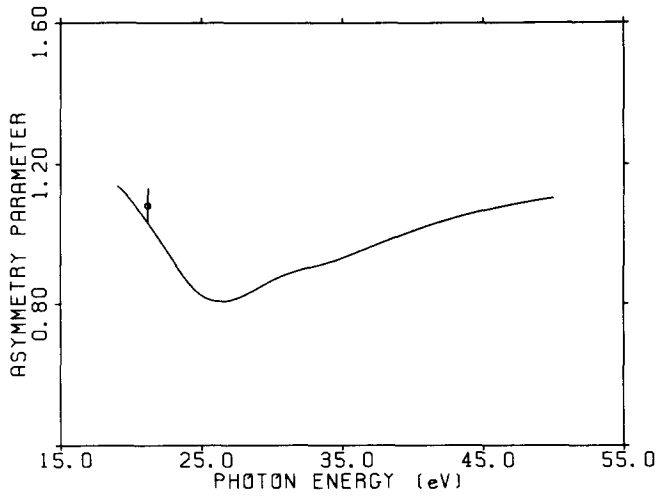

FIG. 12. Photoelectron asymmetry parameters for the $B\,^2\Sigma_u^+$ state of $C_2H_2^+$: —, present results (dipole length form); o, experimental result at 21.22 eV (Ref. 40).

of Figs 8 and 9, respectively. However, the behavior of the eigenphase sum above 35 eV indicates the presence of a broad resonance which does not have any noticeable effect on the calculated vibrationally unresolved cross section or asymmetry parameters. The effect of this broad shape resonance may be more evident in vibrationally resolved cross sections or in photoionization out of lower lying levels.

C. The $B\,^2\Sigma_u^+$ state

In the $B\,^2\Sigma_u^+$ channel photoionization occurs out of the $2\sigma_u$ level into the σ_g and π_g continua. Figure 11 shows the $2\sigma_u \rightarrow k\sigma_g$ and $k\pi_g$ components of this cross section along with their sum, the synchrotron radiation measurements of Unwin and Bradshaw,[20] and the cross sections obtained by the Stieltjes moment theory method.[24] The experimental data has been normalized to our calculated cross sections at a photon energy of 28 eV. The photon energy scale assumes an ionization potential of 18.7 eV.[33]

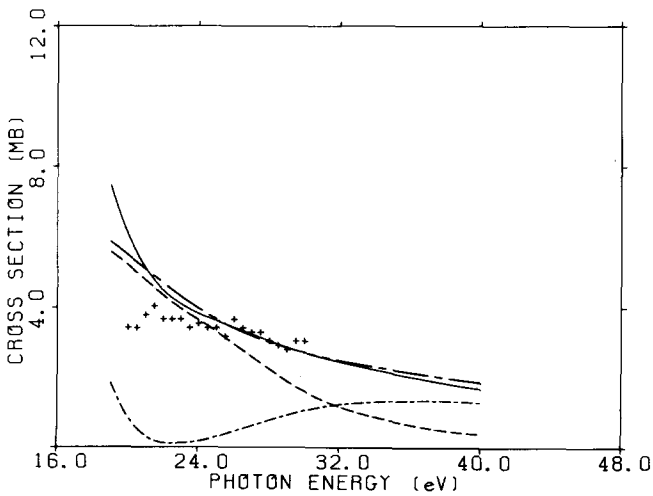

FIG. 11. Photoionization cross sections for the $B\,^2\Sigma_g^+$ state of $C_2H_2^+$: ---, the $2\sigma_u \rightarrow k\sigma_g$ component; – · –, the $2\sigma_u \rightarrow k\pi_g$ component; —, $2\sigma_u$ cross section (dipole length form); — – —, Stieltjes moment theory results (Ref. 24); +, experimental results (Ref. 20) normalized to our cross sections at 28 eV.

From the results of Fig. 11 we see that the calculated cross sections rise too rapidly below 25 eV and are considerably larger than the measured values near threshold. Although this behavior is more pronounced in the σ_g continuum, it is also evident in the π_g cross sections. In contrast the experimental cross sections are quite flat over the range of photon energies in Fig. 11. As suggested previously,[24] this behavior in the $2\sigma_u \rightarrow k\sigma_g$ photoionization cross sections is caused by a discrete valence-like $2\sigma_u \rightarrow n\sigma_g$ transition about 1 eV below ionization which leads to this threshold value. We believe that the similar behavior of the π_g cross sections is probably due to the influence of the intense discrete $2\sigma_u \rightarrow n\pi_g$ transition.[24] We note that in N_2, the calculated $2\sigma_u$ photoionization cross sections did not show these large threshold values in either the σ_g or π_g continuum and, in fact, were quite flat and in good agreement with the measured values.[16] For N_2 the calculated spectrum of excitation frequencies and oscillator strengths[39] does not show any analogous strong $2\sigma_u \rightarrow n\sigma_g$ discrete transition and the relevant intense $2\sigma_u \rightarrow n\pi_g$ transition occurs near 5 eV below threshold, about 2 eV lower than in the case of C_2H_2. Finally, our calculated cross sections are quite similar to those of the Stieltjes moment theory method.[24]

Figure 12 shows the calculated asymmetry parameters for the $2\sigma_u$ level. The behavior of these β values near threshold is again probably influenced by the strong $2\sigma_u \rightarrow n\sigma_g$ transition just below threshold. The single experimental result shown is the value reported for vertical ionization at the HeI line.[40]

D. The $2\sigma_g$ level

For ionization out of this inner-valence region in C_2H_2 and other hydrocarbons, the intensities of satellite bands can be substantial and hence the association of

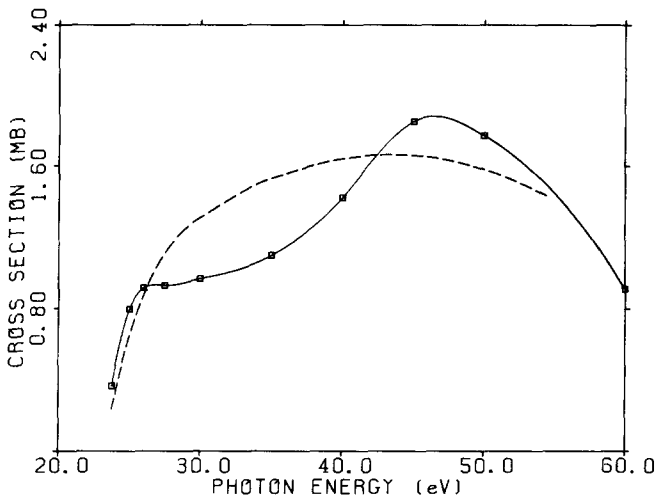

FIG. 13. Cross section for the $(2\sigma_g^{-1})$ $^2\Sigma_g^+$ state of $C_2H_2^+$: —□—, present results (dipole length form); ---, Stieltjes moment theory results (Ref. 24).

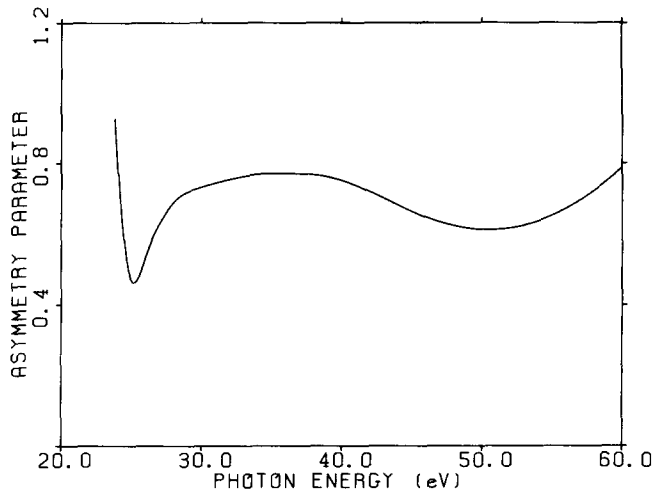

FIG. 15. Photoelectron asymmetry parameters for the $(2\sigma_g^{-1})$ $^2\Sigma_g^+$ state of $C_2H_2^+$.

one spectral line with photoionization out of a particular molecular orbital becomes less valid.[41] Of the two bands at 23.5 and 27.5 eV that can be associated with ionization from the $2\sigma_g$ level, the $2\sigma_g$ ionization potential is assigned to the dominant peak at 23.5 eV.[41] For the present purposes, we will present cross sections assuming that ionization occurs exclusively from the $2\sigma_g$ level. These cross sections display the important characteristics of the electronic continua and can, moreover, be used in conjunction with amplitudes and poles of the one-body Green's function to obtain the correct intensities.[41]

Figure 13 shows the calculated photoionization cross sections for this level along with the results obtained by the STMT method.[24] These cross sections show the enhancement due to the shape resonant behavior of the σ_u continuum around 26 eV and again around 45 eV. From these cross sections, as well as from the associated σ_u eigenphase sums in Fig. 14, we see that the resonance at higher energy is considerably broader than the resonance near threshold. The σ_u eigenphase sum for this channel is quite similar to that of the $3\sigma_g^{-1}$ channel but, whereas the enhancement of the cross section due to the higher energy shape resonance is quite evident for ionization out of the inner-valence $2\sigma_g$ level, no such enhancement is seen in the vibrationally unresolved cross sections for the valence $3\sigma_g$ level. By comparison, the cross sections of the STMT method indicate that this approach has smoothed away the broad double-hump structure in our cross sections caused by these two shape resonances.

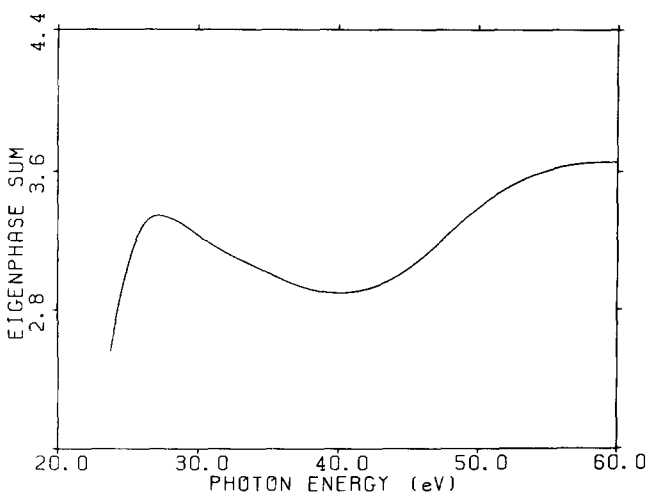

FIG. 14. Eigenphase sum for the $2\sigma_g \rightarrow k\sigma_u$ component.

Figure 15 shows the β parameters for this level calculated in the dipole length approximation. The effect of the near-threshold shape resonance on these β parameters is very evident, whereas there is essentially no effect due to the higher energy resonance. Vibrationally resolved studies of these angular distribution parameters would be useful.

E. The *K* shell

Figure 16 shows the four partial cross sections for photoionization from the $1\sigma_g$ and $1\sigma_u$ K-shell levels. The photon energy scale in this figure assumes an ionization potential of 291.1 eV.[23] The $1\sigma_g$ cross section is dominated by the σ_u shape resonance which has a peak position at about 311 eV. The low energy resonance feature in this continuum seen in the $2\sigma_g$ and $3\sigma_g$ cross sections is no longer present suggesting that the resonance state has moved below threshold. For comparison we also show the values for this $1\sigma_g \rightarrow k\sigma_u$ cross section obtained by the STMT method.[24] The STMT results show a slightly broader resonance feature with a peak value and position shifted to lower values. The $1\sigma_u \rightarrow k\sigma_g$ partial cross section is again relatively large near threshold reflecting the influence of the valence-like $1\sigma_u \rightarrow n\sigma_g$ transition.

The four components of the $1\sigma_g$ and $1\sigma_u$ cross sections of Fig. 16 are combined in Fig. 17 and compared with the measured $(e, 2e)$ intensities for K-shell photo-

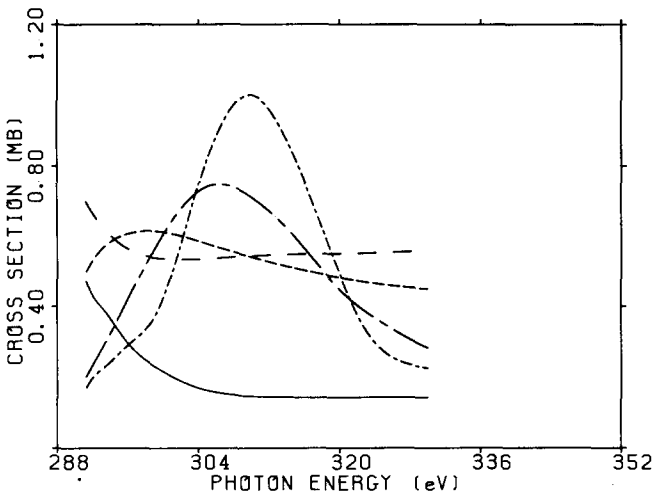

FIG. 16. Calculated partial channel photoionization cross sections for the K shell of $C_2H_2^+$ (dipole length form): ——, $1\sigma_u \rightarrow k\sigma_g$ component; – –, $1\sigma_u \rightarrow k\pi_g$ component; – · –, $1\sigma_g \rightarrow k\sigma_u$ component; — —, $1\sigma_g \rightarrow k\pi_u$ component; — – —, Stieltjes moment theory results for the $1\sigma_g \rightarrow k\sigma_u$ resonant component (Ref. 24).

ionization[23] and with the results of the STMT method.[24] Both sets of calculated intensities were obtained from the corresponding photoionization cross sections.[42] The present results have been normalized to the experimental intensities at 320 eV. Normalization was carried out at 320 eV in order to avoid the threshold region where shakeup effects are evident. Moreover, both sets of calculated cross sections agreed at this energy. A comparison of these cross sections shows that the resonance feature around 310 eV is more pronounced in our results than in both the experimental or STMT intensities. This difference between the calculated intensities comes primarily from the behavior in the $1\sigma_g \rightarrow k\sigma_u$ channel. These differences can be due to the use of too few spectral points in the region of the shape resonance in the STMT studies.[17] Vibrational averaging of these resonant cross sections could broaden these calculated intensities and remove some of the differences between our results and the experimental data in this region. The calculated K-shell asymmetry parameters are shown in Fig. 18. The effects of the shape resonance around 310 eV is clearly evident. No measured values of these parameters have been reported.

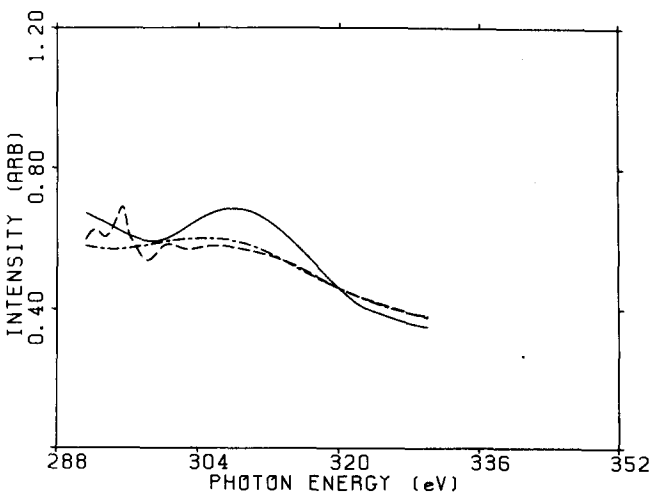

FIG. 17. K-shell photoionization intensities: —, present results normalized to experiment at 320 eV; — · —, Stieltjes moment theory results normalized at threshold (Ref. 24); – – –, experimental results (Ref. 23).

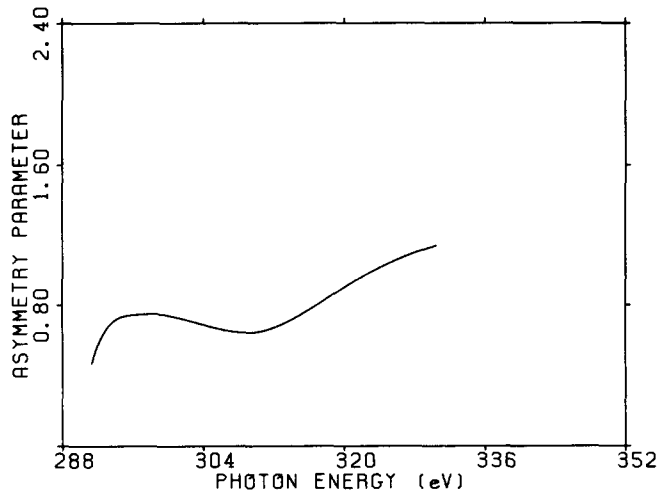

FIG. 18. K-shell photoelectron asymmetry parameters (dipole length form).

IV. CONCLUSION

Accurate fixed-nuclei frozen-core Hartree–Fock photoionization cross sections have been obtained for the valence, inner-valence, and K-shell orbitals of C_2H_2. We have compared these cross sections with available experimental data and with the results of calculations by the STMT method and the multiple scattering approach. These comparisons illustrate the need to obtain photoionization cross sections at the Hartree–Fock continuum level as an initial step in the understanding of molecular photoionization spectra. For example, the present results show that a shape-resonance π_g continuum may play an important role in the $^2\Pi_u(1\pi_u^{-1})$ photoionization cross sections in the same 11–16 eV region where features due to autoionizing resonances are now well established.[6,20] Further clarification of the underlying resonant structure in this spectral region will require studies of these cross sections which include final state correlation effects for both the shape and autoionizing resonances. Absolute measurements of the vibrationally resolved cross sections in this region are needed. Another important conclusion of these studies concerns the behavior of the σ_u continuum where two shape resonances are seen. For ionization out of the $3\sigma_g$ level the lower energy resonance is very pronounced in both the cross sections and asymmetry parameters, whereas the higher energy resonance is not at all evident in these fixed-nuclei results. Vibrationally resolved studies in the region of this higher energy shape resonance would be useful. On the other hand, the effects of both shape resonances are obvious in photoionization out of the inner-valence $2\sigma_g$ level.

ACKNOWLEDGMENTS

One of the authors (VMcK) thanks Wolfgang Domcke for several helpful discussions concerning these results. We also thank Jeffrey Nichols and Danny Yeager for providing us with the results of their calculations on the excitation spectrum of C_2H_2. This material is based upon work supported by the National Science Foundation under Grant No. CHE-8218166. The authors acknowledge computing support from the National Center for Atmospheric Research (NCAR) which is sponsored by the National Science Foundation. The research reported in this paper made use of the Dreyfus–NSF Theoretical Chemistry Computer which was funded through grants from the Camille and Henry Dreyfus Foundation, the National Science Foundation (Grant No. CHE 78-20235), and the Sloan Fund of the California Institute of Technology.

[1]J. B. West, A. C. Parr, B. E. Cole, D. L. Ederer, R. Stockbauer, and J. L. Dehmer, J. Phys. B **13**, L105 (1980).
[2]R. Stockbauer, B. E. Cole, D. L. Ederer, J. B. West, A. C. Parr, and J. L. Dehmer, Phys. Rev. Lett. **43**, 757 (1979).
[3]B. E. Cole, D. L. Ederer, R. Stockbauer, K. Codling, A. C. Parr, J. B. West, E. D. Poliakoff, and J. L. Dehmer, J. Chem. Phys. **72**, 6308 (1980).
[4]T. A. Carlson, M. O. Krause, D. Mehaffy, J. W. Taylor, F. A. Grimm, and J. D. Allen, J. Chem. Phys. **73**, 6056 (1980).
[5]E. W. Plummer, T. Gustafsson, W. Gudat, and D. E. Eastmann, Phys. Rev. A **15**, 2339 (1977).
[6]A. C. Parr, D. L. Ederer, J. B. West, D. M. P. Holland, and J. L. Dehmer, J. Chem. Phys. **76**, 4349 (1982).
[7]J. L. Dehmer, D. Dill, and S. Wallace, Phys. Rev. Lett. **43**, 1005 (1979).
[8]N. Padial, G. Csanak, B. V. McKoy, and P. W. Langhoff, J. Chem. Phys. **69**, 2992 (1978).
[9]R. R. Lucchese and V. McKoy, J. Phys. B **14**, L629 (1981).
[10]R. R. Lucchese and V. McKoy, J. Phys. Chem. **85**, 2166 (1981).
[11]G. Raseev, H. Le Rouzo, and H. Lefebvre-Brion, J. Chem. Phys. **72**, 5701 (1980).
[12]N. Padial, G. Csanak, B. V. McKoy, and P. W. Langhoff, Phys. Rev. A **23**, 218 (1981).
[13]A. Gerwer, C. Asaro, B. V. McKoy, and P. W. Langhoff, J. Chem. Phys. **72**, 713 (1980).
[14]A. E. Orel, T. N. Rescigno, B. V. McKoy, and P. W. Langhoff, J. Chem. Phys. **72**, 1265 (1980).
[15]R. R. Lucchese, D. K. Watson, and V. McKoy, Phys. Rev. A **22**, 421 (1980).
[16]R. R. Lucchese, G. Raseev, and V. McKoy, Phys. Rev. A **25**, 2572 (1982).
[17]R. R. Lucchese and V. McKoy, Phys. Rev. A **26**, 1406 (1982).
[18]M. E. Smith, R. R. Lucchese, and V. McKoy, J. Chem. Phys. **79**, 1360 (1988).
[19]R. R. Lucchese and V. McKoy, Phys. Rev. A **28**, 1382 (1983).
[20]P. W. Langhoff, B. V. McKoy, R. Unwin, and A. Bradshaw, Chem. Phys. Lett. **83**, 270 (1981).
[21]J. Kreile, A. Schweig, and W. Thiel, Chem. Phys. Lett. **79**, 547 (1981).
[22]P. R. Keller, D. Mehaffy, J. W. Taylor, F. A. Grimm, and T. A. Carlson, J. Electron Spectrosc. **27**, 223 (1982).
[23]A. P. Hitchcock and C. E. Brion, J. Electron Spectrosc. **10**, 317 (1977); **22**, 283 (1981).
[24]L. E. Machado, E. P. Leal, G. Csanak, B. V. McKoy, and P. W. Langhoff, J. Electron Spectrosc. **25**, 1 (1982).
[25]P. H. Metzger and G. R. Cook, J. Chem. Phys. **41**, 642 (1964).
[26]R. Unwin, I. Khan, N. V. Richardson, A. M. Bradshaw, L. Cederbaum, and W. Domcke, Chem. Phys. Lett. **77**, 242 (1981).
[27]R. R. Lucchese and V. McKoy, XII International Conference on the Physics of Electronic and Atomic Collisions, Book of Abstracts, July 15–21, 1981, Gatlinburg, Tennessee, p. 80.
[28]T. N. Rescigno, A. Gerwer, B. V. McKoy, and P. W. Langhoff, Chem. Phys. Lett. **66**, 116 (1979).
[29]R. R. Lucchese and V. McKoy, Phys. Rev. A **24**, 770 (1981).
[30]See, for example, W. H. Miller, J. Chem. Phys. **50**, 407 (1969).
[31]T. H. Dunning and P. J. Hay, in *Modern Theoretical Chemistry* 3, edited by H. F. Schaefer III (Plenum, New York, 1977), p. 1.
[32]J. R. Swanson and J. L. Armstrong, Jr., Phys. Rev. A **15**, 661 (1977).
[33]D. W. Turner, C. Baker, A. D. Baker, and C. B. Brundle, *Molecular Photoelectron Spectroscopy* (Wiley, New York, 1970).
[34]Z. H. Levine and P. Soven, Phys. Rev. Lett. **50**, 2074 (1983).
[35]S. Trajmar, J. K. Rice, P. S. P. Wei, and A. Kuppermann, Chem. Phys. Lett. **1**, 703 (1968).
[36]J. Nichols and D. L. Yeager (private communication).
[37]W. C. Walker and G. L. Weissler, J. Chem. Phys. **23**, 1547 (1955).
[38]R. I. Schoen, J. Chem. Phys. **37**, 2032 (1962).
[39]T. N. Rescigno, C. F. Bender, B. V. McKoy, and P. W. Langhoff, J. Chem. Phys. **68**, 970 (1978).
[40]J. Kreile and A. Schweig, Chem. Phys. Lett. **69**, 71 (1980).
[41]A. M. Bradshaw, W. Eberhardt, H. J. Levinson, W. Domcke, and L. S. Cederbaum, Chem. Phys. Lett. **70**, 36 (1980).
[42]M. Inokuti, Rev. Mod. Phys. **43**, 297 (1978).